RESEARCH ARTICLE | DECEMBER 19 2025

Experimental determination of equilibrium stress in stress-induced martensitic transformation at low temperatures in Ni-rich TiNi

Kodai Niitsu ; Ryosuke Kainuma

Appl. Phys. Lett. 127, 241903 (2025)
https://doi.org/10.1063/5.0301524

Applied Physics Letters ARTICLE pubs.aip.org/aip/apl

Experimental determination of equilibrium stress in stress-induced martensitic transformation at low temperatures in Ni-rich TiNi

Cite as: Appl. Phys. Lett. **127**, 241903 (2025); doi: 10.1063/5.0301524
Submitted: 9 September 2025 · Accepted: 4 December 2025 ·
Published Online: 19 December 2025

Kodai Niitsu[1,a] and Ryosuke Kainuma[2]

AFFILIATIONS

[1]Center for Basic Research on Materials, National Institute for Materials Science (NIMS), Tsukuba, Ibaraki 305-0047, Japan
[2]Department of Materials Science, Graduate School of Engineering, Tohoku University, Sendai 980-8579, Japan

[a]Author to whom correspondence should be addressed: NIITSU.Kodai@nims.go.jp. Tel.: +81-29-859-2566

ABSTRACT

The exceptional broadening of superelastic stress hysteresis at low temperatures in Ni-rich Ti–Ni shape-memory alloys impedes their cryogenic applications. This broadening arises from thermally activated habit plane glide. Traditionally, equilibrium stress has been assumed to lie at the midpoint between forward and reverse martensitic transformation (MT) stresses, assuming reciprocal kinetics. Here, we assess this assumption using strain-rate jump tests, a simple method that detects the magnitude of stress change in response to strain-rate variation. The observed stress change is consistently larger during the forward MT than the reverse MT, indicating an asymmetric thermal activation and a shift in equilibrium stress toward the reverse MT stress. This result deviates from the classical midpoint approximation in systems with significant hysteresis broadening. Strain-rate jump test is demonstrated to be a simple yet effective method for locating the equilibrium stress, even when it is bracketed deep within a broadened stress hysteresis.

Shape-memory alloys (SMAs) are a class of alloys that undergo a diffusionless solid–solid phase transformation known as martensitic transformation (MT). Their hallmark functionalities—the shape-memory effect and superelasticity—have long attracted significant attention in the field of materials science and engineering.[1,2] Among them, Nitinol, a Ti–Ni-based alloy has served as a benchmark SMA owing to its good cold-workability and prominent fatigue resistance, enabling its widespread application at temperatures above ambient.[3–8] At low temperatures, however, these functionalities become difficult to operate due to the pronounced broadening of the transformation hysteresis.[9] This hysteresis broadening originates from the thermally activated glide of habit planes.[10] A kinetic description of thermally activated habit plane glide extensively explains the viscous nature of low-temperature MTs,[11] which is manifested as the isothermal MT,[12–14] the kinetic arrest,[15] the strain glass behavior (vanishing MT),[16] and the broken ergodicity.[17]

The extent to which the low-temperature MT dynamics is governed by thermal activation is material-dependent. A characteristic measure is the 0 K-extrapolated thermal activation component of the stress hysteresis, which informs the intrinsic barrier associated with thermal activation. Reported values vary widely across alloy systems: 747–1074 MPa in a Ni-rich Ti–Ni,[9–11] 628 MPa in a Ti–Ni–Cu,[18] ∼1150 MPa in a nanocrystalline Ti–Ni–Fe,[19] ∼480 MPa in a Ti–Al–Cr,[20] 125 MPa in a Co–Cr–Al–Si,[21] 110 MPa in a Ni–Co–Mn–In,[22] and ∼0 MPa in a Cu–Al–Mn[23] and a Fe–Mn–Al–Cr–Ni.[24] Among these, Ni-rich Ti–Ni exhibits exceptionally significant thermal activation, making its low-temperature operation particularly challenging. To uncover the nature of this pronounced thermal activation in this system, it is essential to decompose the total hysteresis into its components to drive the habit plane forward and backward—in other words, to determine the equilibrium stress.

A widely used approximation assumes that thermodynamic equilibrium is achieved at the midpoint between the start temperature of the forward MT (T_M) and the finish temperature of the reverse MT (T_A).[25] This approximation has been extended to other external variables—stress, magnetic field, and composition—and is often treated as self-evident. However, are these approximations truly valid—and if so, to what extent? This question may appear trivial at temperatures above the ambient temperature, where the thermally activated nature of the MT is fully diminished and vibrational entropy shows little temperature dependence. At lower temperatures, however, where the thermal activation becomes pronounced and vibrational entropy notably depends on temperature, the validity of such approximations may warrant scrutiny.

Indeed, this concern has been examined for the case of metamagnetic (magnetic field-induced) MTs in a Ni–Co–Mn–In alloy,[26] revealing that the equilibrium magnetic field is biased toward the field required to complete the reverse MT. This suggests that the thermal activation nature is more pronounced in the forward MT than in the reverse MT. A similar trend has also been confirmed in a system exhibiting a magnetic field-induced first-order ferrimagnetic–antiferromagnetic transformation with substantial hysteresis broadening.[27] In these studies, the equilibrium magnetic field was estimated by measuring the specific heat under different static magnetic fields, while the critical fields for the forward and reverse transformations were determined by sweeping the field. This approach requires the stabilization of single-phase states of both competing phases within the temperature window of interest; thus, specific heat measurements are performed under different static magnetic fields. For stress-induced MTs, however, this approach is not feasible as performing specific heat measurements under uniaxial stress remains technically challenging.

To locate the equilibrium stress bracketed by the stress hysteresis, we performed a strain-rate jump test. This technique is commonly employed to evaluate the activation volume associated with dislocation glide during plastic deformation. In this sense, the change in superelastic flow stress in response to a strain-rate jump is a direct measure of the manifestation of thermally activated habit plane glides. Even better, this method allows simultaneous extraction of the equilibrium stress and the critical stresses for starting/finishing the forward/reverse MTs with a single test. Applying this method to a benchmark Ni-rich Ti–Ni, an essential difference in the thermal activation characteristics of the forward and reverse MTs can be disclosed.

A Ti–51.7Ni (at.%) alloy was fabricated by arc melting. At this composition, thermally induced MT is completely suppressed in the absence of external stress.[9] The as-cast polycrystalline button was homogenized at 1173 K for 24 h, followed by quenching in water. A $2.5 \times 2.5 \times 7.0$-mm specimen was cut from the button for mechanical testing. The specimen is polycrystalline with an average radius of approximately 18 μm containing small amounts of intergranular Ti_4Ni_2O inclusions, the microstructure of which is presented in the supplementary material, Sec. S1. Compression tests were conducted over the temperature range of 20–180 K and strain rates ranging from 1.2×10^{-6} to 5.0×10^{-2} s^{-1}. Strain-rate jump tests were performed between 5.0×10^{-4} and 5.0×10^{-5} s^{-1} at a strain interval of approximately 0.3%–0.4%. It has been confirmed that a steady state is reached within several seconds ($< 0.1\%$ in strain) after the strain rate changes. It is important to note that these strain rates were selected to obtain an apparent response of flow stress while sufficiently reducing any thermal effects. According to our previous study,[10] it is recommended that strain-rate tests be performed in the range of 10^{-6}–10^{-3} s^{-1}. Strain was recorded by an extensometer attached to the compression jigs, with a sampling rate of 1000 Hz. We note that all mechanical tests were conducted on a single specimen. Functional fatigue of superelasticity[28] tested on another rectangular specimen is presented in the supplementary material, Sec. S2. The overall change in critical stresses during the successive 11 cycles, which is required for obtaining the temperature-variable stress–strain curves, does not exceed 25 MPa, which is small enough compared to the intrinsic temperature dependence of the critical stresses.

Figure 1(a) presents the stress–strain curves obtained from the strain-rate jump tests. Strain-rate jumps were repeatedly applied

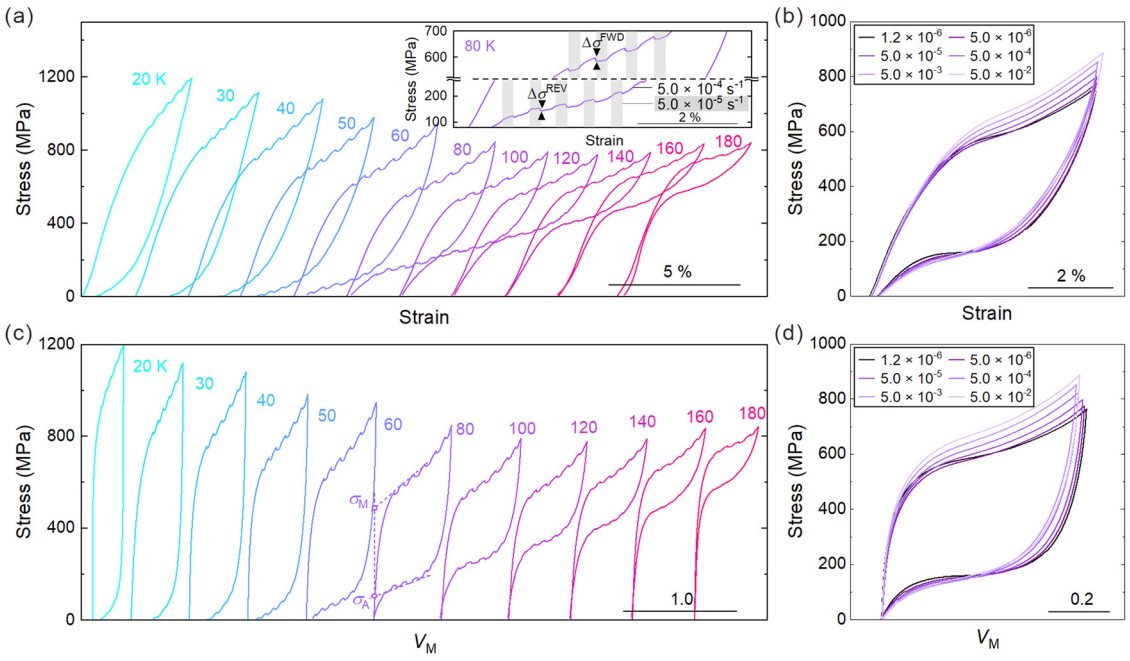

FIG. 1. Superelastic behaviors at various temperatures and strain rates. (a) Stress–strain curves obtained from strain-rate jump tests. The strain rate was initially set at 5.0×10^{-4} s^{-1} and intermittently reduced to 5.0×10^{-5} s^{-1} during both the forward and reverse superelastic flow (see inset). (b) Stress–strain curves obtained at constant strain rates ranging from 1.2×10^{-6} to 5.0×10^{-2} s^{-1} at 80 K. (c) and (d) Stress–V_M (martensite volume fraction) relationships converted from the data in (a) and (b), respectively.

during both the forward and reverse superelastic flow, as highlighted in the inset of Fig. 1(a). This test was carried out sequentially from 180 K down to lower temperatures. Note that the residual, unrecovered superelastic strain, which becomes pronounced below 80 K due to hysteresis broadening, was fully recovered by subsequent annealing above 100 K. The hysteresis broadening with decreasing temperature is a straightforward manifestation of the thermally activated nature of habit plane glide. As shown in the inset of Fig. 1(a), the change (in absolute value) in forward superelastic flow stress, $\Delta\sigma^{\mathrm{FWD}}$, in response to the strain-rate change from 5.0×10^{-4} to 5.0×10^{-5} s^{-1} is downward, which follows the same trend typically observed in dislocation glides; but the counterpart in the reverse flow, $\Delta\sigma^{\mathrm{REV}}$, is upward.

As elucidated in our previous studies, the thermal activation of habit plane glide is manifested not only in the temperature dependence of stress hysteresis but also in the strain-rate dependence of stress hysteresis[10] and the isothermal development of the forward and reverse MTs.[11] At 80 K, compression tests were performed at various constant strain rates, and the resulting stress–strain curves are presented in Fig. 1(b). The forward and reverse superelastic flow stresses exhibit monotonic trends with strain rate: the forward stress decreases, while the reverse stress increases with decreasing strain rate. These opposing trends persist throughout the tested strain-rate range; however, their magnitudes appear to differ. Although temperature fluctuations due to the thermal effects should be taken into account at higher strain rates, the result sheds light on a potential inequivalence in the degree of thermal activation governing the forward and reverse habit plane glides.

The magnitude of superelastic (anelastic) strain is a direct measure of the volume fraction of transformed martensite V_{M}. Nevertheless, the strain in the experimental stress–strain curve involves the superelastic strain as well as the elastic strain of the parent and martensite phases, and thus conveys less information on the evolution of MTs. The stress–strain curves in Figs. 1(a) and 1(b) were converted to stress–V_{M} curves, as shown in Figs. 1(c) and 1(d), respectively, where the details of this mathematical conversion are described in the supplementary material, Sec. S3. The critical stresses $\sigma_{\mathrm{M}}/\sigma_{\mathrm{A}}$ for starting/finishing the forward/reverse MTs are defined as the intercepts at $V_{\mathrm{M}}=0$ of the linear extrapolations of the forward and reverse superelastic plateaus, as illustrated in Fig. 1(c). They are plotted in Fig. 3(c) as a function of temperature, the discussion of which will be given later.

The results of strain-rate jump tests provide detailed insights into the thermally activated dynamics of MTs. The values of $\Delta\sigma^{\mathrm{FWD}}$ and $\Delta\sigma^{\mathrm{REV}}$, arbitrarily obtained at various levels of V_{M}, are presented in the bottom panels of Figs. 2(a) and 2(b), respectively. These values are dependent on V_{M}, as well as temperature. In the case of dislocation glides, the magnitude of shear stress drop in response to a strain-rate jump depends on accumulated plastic strain, reflecting interactions between moving dislocations and evolving substructures or themselves. Therein, in BCC metals, the stress drop typically increases with

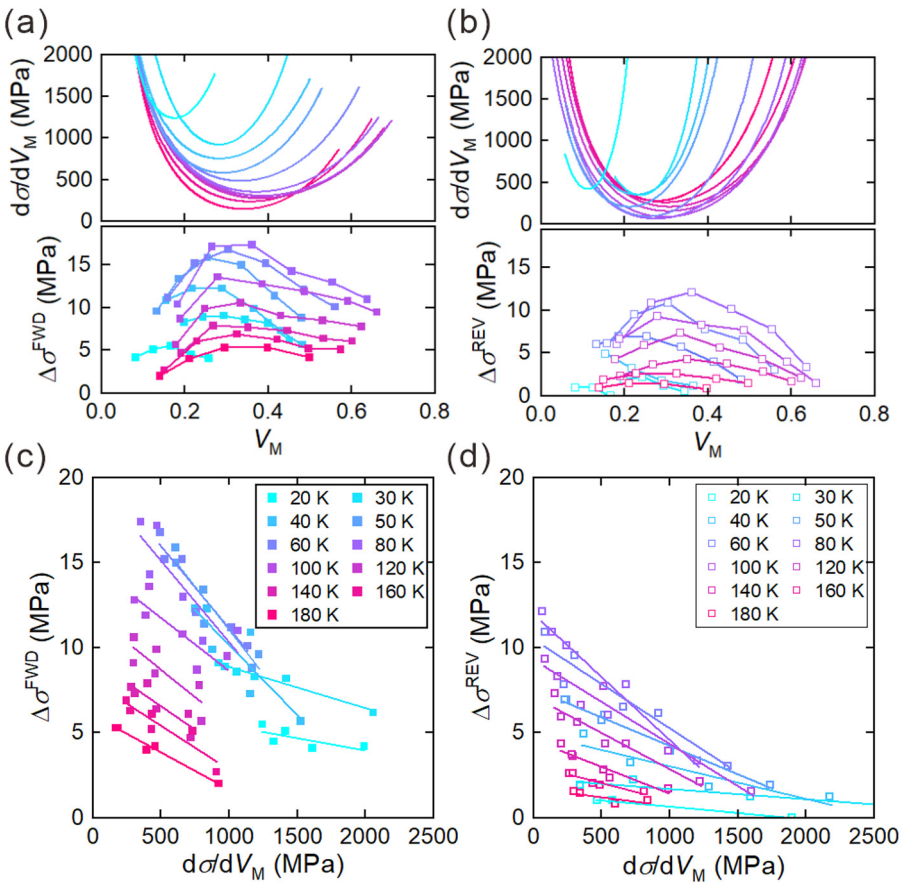

FIG. 2. Scalability of the stress change amplitude $\Delta\sigma^{\mathrm{FWD/REV}}$. Top panels: Temperature-dependent profiles of $\mathrm{d}\sigma/\mathrm{d}V_{\mathrm{M}}$ during the forward (a) and reverse (b) strain flows. Bottom panels: Plots of $\Delta\sigma^{\mathrm{FWD}}$ (a) and $\Delta\sigma^{\mathrm{REV}}$ (b) as a function of V_{M}, extracted from the strain-rate jump tests. $\mathrm{d}\sigma/\mathrm{d}V_{\mathrm{M}}$ are obtained from the mathematically fitted σ–V_{M} curves (see Fig. S3). Rescaled plots of $\Delta\sigma^{\mathrm{FWD}}$ (c) and $\Delta\sigma^{\mathrm{REV}}$ (d) as a function of $\mathrm{d}\sigma/\mathrm{d}V_{\mathrm{M}}$, showing linear correlations at respective temperatures.

increasing plastic strain, which corresponds to a reduction in activation volume due to dislocation forest hardening. In contrast, $\Delta\sigma^{FWD}$ and $\Delta\sigma^{REV}$ show non-monotonic variations with V_M (analogous to the superelastic strain), reaching maxima near the point where the superelastic-hardening rate [identical to $d\sigma/dV_M$, see top panels of Figs. 2(a) and 2(b)] reaches a minimum. This behavior suggests that the magnitude of $\Delta\sigma^{FWD}$ and $\Delta\sigma^{REV}$ is uniquely scalable with the density of mobile habit planes. This interpretation is plausible given that habit planes do not intersect and the displacive atomic shear at the transformation front is likely less influenced by interfacial interactions, unlike dislocations. The relationship between $\Delta\sigma^{FWD/REV}$ and $d\sigma/dV_M$ is plotted in Figs. 2(c) and 2(d), showing linear correlation at each temperature.

$\Delta\sigma^{FWD}$ and $\Delta\sigma^{REV}$ are now confirmed to scale with the density of mobile habit planes. To be compared as a function of temperature, their extrapolated values at $d\sigma/dV_M = 0$, herein referred to as $\Delta\sigma_{off}^{FWD}$ and $\Delta\sigma_{off}^{REV}$, were estimated via linear fits, as presented in Fig. 3(a). They reach maxima under conditions where the habit planes become thermally mobile yet remain significantly arrested within the timescale imposed by the given strain rate. Most importantly, $\Delta\sigma_{off}^{REV}$ is consistently smaller than $\Delta\sigma_{off}^{FWD}$ across the entire temperature range tested, and their peak temperatures differ. These findings highlight the different characteristics and magnitude of thermal activation processes involved in the forward and reverse MT pathways.

To elucidate the different dynamics of the forward and reverse MTs, the overall hysteresis σ_{hys} was decomposed into effective components associated with each MT pathway, σ_{eff}^{FWD} and σ_{eff}^{REV}, such that

$$\sigma_{hys} = \sigma_{eff}^{FWD} + \sigma_{eff}^{REV}. \quad (1)$$

They were further decomposed into athermal and isothermal terms such that

$$\sigma_{eff} = \sigma_{\mu} + \sigma_{TA}\left[1 - \left\{\frac{k_B T}{\Delta H_0}\ln\left(\frac{\dot{\varepsilon}_0}{\dot{\varepsilon}_{SE}}\right)\right\}^{1/q}\right]^{1/p}, \quad (2)$$

where σ_{μ} and σ_{TA} represent the athermal component and the 0 K thermal activation offset for the overloading/underloading stresses required to drive the forward/reverse MTs, respectively; ΔH_0 is the activation enthalpy at 0 K; k_B is the Boltzmann constant; $\dot{\varepsilon}_0$ is a pre-exponential factor; $\dot{\varepsilon}_{SE}$ is the superelastic strain rate; and p and q are adjustable parameters that shape the tail and top of the obstacle profile.[10] The ranges of p and q are restricted to $0 < p \leq 1$ and $1 \leq q \leq 2$ to guarantee that the activation area increases continuously as the applied stress decreases.[29,30] Subscripts "FWD" and "REV" are omitted in Eq. (2), but the parameters were independently determined for the forward and reverse MTs. Since $\Delta\sigma_{off}^{FWD/REV}$ is identical to the difference in $\sigma_{eff}^{FWD/REV}$ at $\dot{\varepsilon}_{SE} = 5.0 \times 10^{-4}$ and 5.0×10^{-5} s^{-1}, the fitting to

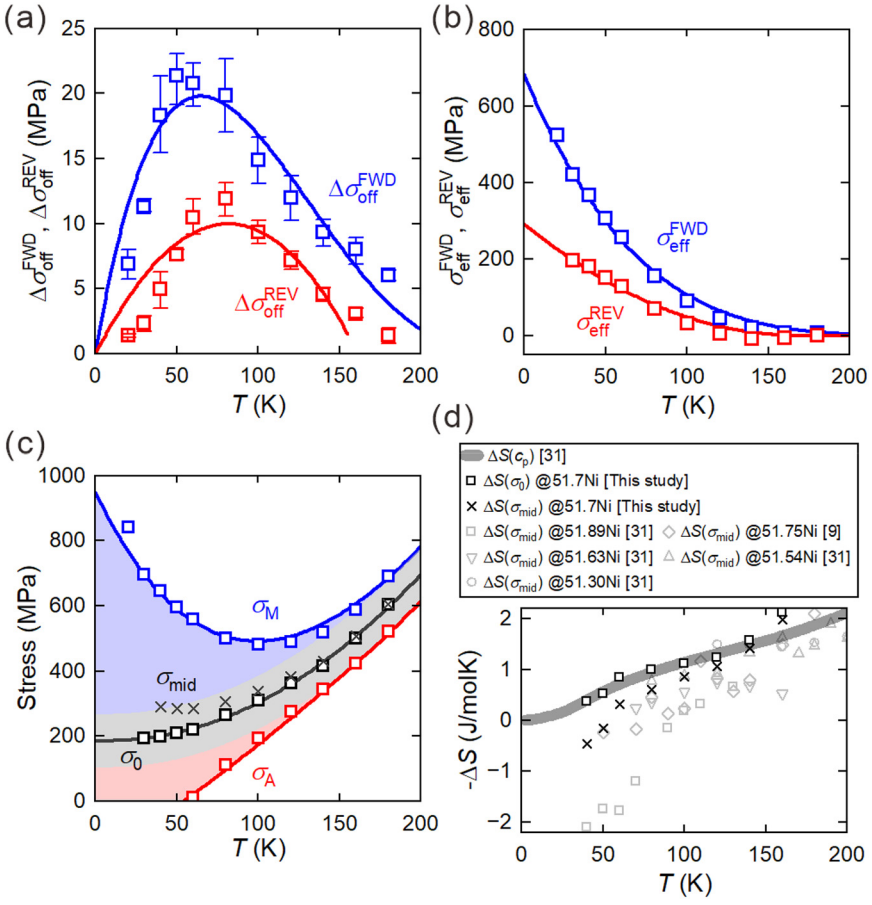

FIG. 3. Decomposition of transformation hysteresis and determination of equilibrium stress. (a) Temperature dependence of the extrapolated stress drop offsets, $\Delta\sigma_{off}^{FWD}$ and $\Delta\sigma_{off}^{REV}$, derived from the data in Figs. 2(c) and 2(d). The solid curves represent least squares fits using Eq. (2). (b) Temperature dependence of the effective stresses for driving the forward and reverse MTs, σ_{eff}^{FWD} and σ_{eff}^{REV} at $\dot{\varepsilon}_{SE} = 5.0 \times 10^{-5}$ s^{-1}, derived using Eq. (2) with parameters tabulated in Table I. (c) Stress–temperature phase diagram involving equilibrium stress σ_0, forward/reverse MT starting/finishing stresses σ_M/σ_A, and their midpoint σ_{mid}. (d) Entropy change ΔS estimated using σ_0 and σ_{mid} and from specific heat measurements.

$\Delta\sigma_{off}^{FWD/REV}$ plots can performed by least squares fitting using Eq. (2). The resultant fitting curves are presented in Fig. 3(a) and the values of the parameters used are listed in Table I.

Using the derived parameters, σ_{eff}^{FWD} and σ_{eff}^{REV} can be independently exploited; as a representative example, their temperature functions at $\dot{\varepsilon}_{SE} = 5.0 \times 10^{-5}\ s^{-1}$ are shown in Fig. 3(b). This presentation clearly shows that the transformation hysteresis is shaped by the different magnitudes of thermal activation between the forward and reverse MTs. The thermal activation offset at 0 K for the forward MT, σ_{TA}^{FWD}, is approximately 2.3 times greater than that of the reverse MT, σ_{TA}^{REV}. Furthermore, the thermal activation persists up to a higher limiting temperature for the forward MT, 270 K $\left[= \frac{\Delta H_0}{k_B} \ln\left(\frac{\dot{\varepsilon}_{SE}}{\dot{\varepsilon}_0}\right)\right]$, compared to 166 K for the reverse MT. The athermal component σ_μ was estimated under the assumption ${\sigma_\mu}^{FWD} = {\sigma_\mu}^{REV}$ $(\equiv \sigma_\mu)$. Although this approximation is not self-evident, it has been demonstrated to be reasonable based on thermodynamic analysis in a Ni–Co–Mn–In metamagnetic SMA.[26]

Once all components of σ_{hys} are broken down, σ_0 can be determined such that the following factor Δ is minimized:

$$\Delta = \left\{\sigma_M - \left(\sigma_0 + \sigma_{eff}^{FWD}\right)\right\}^2 + \left\{\sigma_A - \left(\sigma_0 - \sigma_{eff}^{REV}\right)\right\}^2. \quad (3)$$

The resultant σ_0 values are plotted in Fig. 3(c), alongside σ_M, σ_A, and their midpoint σ_{mid}. The black curve represents a polynomial fit to the σ_0 plots. The blue and red curves correspond to $\sigma_0 + \sigma_{eff}^{FWD}$ and $\sigma_0 - \sigma_{eff}^{REV}$, respectively. They closely trace the experimental σ_M and σ_A plots, corroborating that the mathematical handling of the results of the strain-rate jump tests makes sense. The deviation of σ_0 from σ_{mid} becomes pronounced, and σ_0 biases toward σ_A with decreasing temperature. This trend is consistent with previous investigations of a metamagnetic MT in Ni–Co–Mn–In[26] and a first-order ferrimagnetic-to-antiferromagnetic transition in $(Fe_{0.95}Zn_{0.05})_2Mo_3O_8$,[27] both of which exhibit substantial hysteresis broadening. We note that this biasing enables better reproduction of the different isothermal dynamics observed between the forward and reverse MT pathways, as discussed in Ref. 11.

A straightforward benefit of properly assessing σ_0 is that it enables an accurate evaluation of entropy change ΔS, which can be calculated by the Clausius–Clapeyron equation given by

$$\frac{\partial \sigma_0}{\partial T} = -\frac{\Delta S}{\varepsilon_{SE} V_m}, \quad (4)$$

where ε_{SE} is the full superelastic strain $(= 0.055$[11]$)$ and ΔS is generally estimated using the traditional approximation $\sigma_{mid} = \sigma_0$. However, as shown in Fig. 3(d), this approximation is not reliable at lower temperatures, eventually resulting in a sign reversal of ΔS.[9,31] This study is no exception, and ΔS derived using σ_{mid} reverses its sign below 50 K. Alternatively, ΔS evaluated using σ_0 can better reproduce the ΔS curve obtained directly from specific heat measurements.[31]

TABLE I. Fitting parameters used in Eq. (2) for the forward and reverse MTs.

	σ_μ (MPa)	σ_{TA} (MPa)	ΔH_0 (eV)	$\dot{\varepsilon}_0$ (s^{-1})	p	q
Forward MT	82	682	0.74	4.0×10^{10}	0.25	1.01
Reverse MT	82	291	0.47	7.6×10^{10}	0.51	1.00

In the realm of MT dynamics driven by thermally activated processes, it is revealed that the transformation stress hysteresis is shaped by inequivalent magnitudes of excess stresses for forwarding and reverting habit planes. This result, in conjunction with previous findings,[26,27] strongly suggests that a larger driving force is required for the transforming interface to propagate into the high-temperature parent phase. The kinetic driving force is scaled by the non-chemical free energy, which is primarily dictated by interfacial energy. Among various contributions, the stored elastic energy is considered a dominant source for the present case. According to Kocks *et al.*,[30] the adjustable parameters, p and q, in Eq. (2) inform the glide resistance over obstacles. The smaller p value for the forward MT suggests that a longer-range glide resistance acts during the propagation of the habit plane into the parent $B2$ phase. A promising source of the glide resistance is the internal stress arising from lattice mismatch. Indeed, James and co-workers have revealed that highly compatible lattice correspondences can dramatically reduce thermal hysteresis.[32–34] However, this context is, we think, primarily valid for the athermal component of hysteresis and insufficient to explain the inequivalent driving forces. The possible differences in the generation or annihilation processes of long-range lattice defects (such as dislocations and stacking faults) in the forward and reverse MTs may be the origin of the observed non-reciprocal thermal activation.

The classical approximation for the thermodynamic equilibrium temperature,[25] $T_0 = (T_M + T_A)/2$, is reevaluated here based on Fig. 3(c). T_M and T_A are defined as the temperatures intersecting the σ_M and σ_A lines during cooling and heating, respectively, under a given static stress. Under a high static stress (e.g., $>$ 600 MPa), where both T_M and T_A are largely athermal, the midpoint approximation holds reasonably. However, as the static stress decreases, the thermal activation component becomes increasingly pronounced especially for the forward MT, leading to a deviation of T_0 from the midpoint. Most notably, there exists a stress range (approximately 200–450 MPa) in which T_M is not detectable, yet T_0 remains well defined. This arises from the pronounced time-dependent thermal activation. Hence, the midpoint approximation is only valid in regimes dominated by athermal hysteresis. (Strictly speaking, differences in entropy changes at T_M and T_A disturb this approximation, even if fully athermal.) The same context can be applied to equilibrium stress, magnetic field, and composition, as the vertical axis of Fig. 3(c) can be converted analogously to magnetic field and composition.[35]

To summarize, strain-rate jump tests were performed in this study to locate the equilibrium stress for the stress-induced MTs in a Ni-rich Ti–Ni alloy. Despite significant hysteresis broadening, the equilibrium stress could be determined and the assessed phase diagram reveals that the transformation hysteresis is shaped by different degrees of thermal activation between the forward and reverse MTs. The commonly employed assumption that thermodynamic equilibrium lies at the midpoint of the transformation hysteresis becomes increasingly invalid with lowering temperature. Our results indicate that the forward MT requires a greater kinetic driving force than the reverse MT, shedding light on the non-reciprocal propagation behavior of the habit plane.

See the supplementary material for additional details on microstructural characterization, cyclic fatigue of superelasticity, and the mathematical conversion of stress–strain curves.

The authors thank Dr. Oike and Dr. Suyama for helpful discussions and technical assistance. This study was supported by JST PRESTO (Grant No. JPMJPR22Q6) and JSPS KAKENHI (Grant Nos. 23K04366 and 19H02418).

AUTHOR DECLARATIONS

Conflict of Interest

The authors have no conflicts to disclose.

Author Contributions

Kodai Niitsu: Conceptualization (equal); Data curation (equal); Formal analysis (equal); Funding acquisition (equal); Investigation (equal); Methodology (equal); Project administration (equal); Resources (equal); Validation (equal); Visualization (equal); Writing – original draft (equal); Writing – review & editing (equal). **Ryosuke Kainuma:** Supervision (equal); Validation (equal); Writing – original draft (equal); Writing – review & editing (equal).

DATA AVAILABILITY

The data that support the findings of this study are available from the corresponding author upon reasonable request.

REFERENCES

[1]V. Raghavan, *Martensite* (ASM International, Materials Park, OH, 1992).
[2]K. Otsuka and C. M. Wayman, *Shape Memory Materials* (Cambridge University Press, United Kingdom, 1998).
[3]N. B. Morgan, "Medical shape memory alloy applications—The market and its products," Mater. Sci. Eng., A **378**, 16 (2004).
[4]J. M. Jani, M. Leary, A. Subic, and M. A. Gibson, "A review of shape memory alloy research, applications and opportunities," Mater. Des. **56**, 1078 (2014).
[5]S. Alipour, F. Taromian, E. R. Ghomi, M. Zare, S. Singh, and S. Ramakrishna, "Nitinol: From historical milestones to functional properties and biomedical applications," Proc. Inst. Mech. Eng., Part H **236**, 1595 (2022).
[6]M.-S. Kim, J.-K. Heo, H. Rodrigue, H.-T. Lee, S. Pane, M.-W. Han, and S.-H. Ahn, "Shape memory alloy (SMA) actuators: The role of material, form, and scaling effects," Adv. Mater. **35**, 2208517 (2023).
[7]Y. Zhang, D. Wei, Y. Chen, L. Xie, L. Wang, L.-C. Zhang, W. Lu, and G. Chen, "Non-negligible role of gradient porous structure in superelasticity deterioration and improvement of NiTi shape memory alloys," J. Mater. Sci. Technol. **186**, 48 (2024).
[8]W. Liu, Y. Zhang, B. Wang, S. Liu, Y. Wang, L. Zhang, L. Zhang, L.-C. Zhang, W. Lu, and L. Wang, "Achieving excellent strength-ductility-superelasticity combination in high-porosity NiTiNb scaffolds via high-temperature annealing," J. Mater. Sci. Technol. **206**, 221 (2025).
[9]K. Niitsu, T. Omori, and R. Kainuma, "Stress-induced transformation behaviors at low temperatures in Ti-51.8 Ni (at.%) shape memory alloy," Appl. Phys. Lett. **102**, 231915 (2013).
[10]K. Niitsu, H. Date, and R. Kainuma, "Thermal activation of stress-induced martensitic transformation in Ni-rich Ti-Ni alloys," Scr. Mater. **186**, 263 (2020).
[11]K. Niitsu, Y. Yano, R. Kainuma, and H. Inui, "Viscosity of superelasticity: A comprehensive interpretation of nonreciprocal isothermal dynamics, kinetic arrest, and nonergodic anelastic strain based on thermal activation of martensitic transformations," Phys. Rev. B **108**, 134103 (2023).
[12]G. V. Kurdjumov and O. P. Maksimova, "Kinetics of austenite-to-martensite transformation at low temperatures," Dokl. Akad. Nauk SSSR **61**, 83 (1948).
[13]G. V. Kurdjumov and O. P. Maksimova, "Work required in the formation of martensite nuclei," Dokl. Akad. Nauk SSSR **73**, 95 (1950).
[14]C. H. Shih, B. L. Averbach, and M. Cohen, "Some characteristics of the isothermal martensitic transformation," Trans. Metall. Soc. AIME **7**, 183 (1955).
[15]W. Ito, K. Ito, R. Y. Umetsu, and R. Kainuma, "Kinetic arrest of martensitic transformation in the NiCoMnIn metamagnetic shape memory alloy," Appl. Phys. Lett. **92**, 021908 (2008).
[16]X. Ren, Y. Wang, Y. Zhou, Z. Zhang, D. Wang, G. Fan, K. Otsuka, T. Suzuki, Y. Ji, J. Zhang, Y. Tian, S. Hou, and X. Ding, "Strain glass in ferroelastic systems: Premartensitic tweed versus strain glass," Philos. Mag. **90**, 141 (2010).
[17]Y. Wang, X. Ren, K. Otsuka, and A. Saxena, "Evidence for broken ergodicity in strain glass," Phys. Rev. B **76**, 132201 (2007).
[18]Y. Kimura, X. Xu, K. Niitsu, T. Omori, and R. Kainuma, "Martensitic transformations and superelastic behavior at low temperatures in $Ti_{50-x}Ni_{40+x}Cu_{10}$ shape memory alloys," Mater. Trans. **57**, 269 (2016).
[19]Q. Li, Y. Chen, Y. Liu, D. Jiang, Y. Yang, H. Yang, K. Yu, Y. Ren, and L. Cui, "Non-linear temperature dependences of pseudoelastic stress and stress hysteresis of a nanocrystalline $Ni_{47}Ti_{50}Fe_3$ alloy," Acta Mater. **265**, 119625 (2024).
[20]Y. Song, S. Xu, S. Sato, I. Lee, X. Xu, T. Omori, M. Nagasako, T. Kawasaki, R. Kiyanagi, S. Harjo, W. Gong, T. Grabec, P. Stoklasová, and R. Kainuma, "A lightweight shape-memory alloy with superior temperature-fluctuation resistance," Nature **638**, 965 (2025).
[21]T. Odaira, S. Xu, X. Xu, T. Omori, and R. Kainuma, "Elastocaloric switching effect induced by reentrant martensitic transformation," Appl. Phys. Rev. **7**, 031406 (2020).
[22]K. Niitsu, X. Xu, R. Y. Umetsu, and R. Kainuma, "Stress-induced transformations at low temperatures in a $Ni_{45}Co_5Mn_{36}In_{14}$ metamagnetic shape memory alloy," Appl. Phys. Lett. **103**, 242406 (2013).
[23]K. Niitsu, Y. Kimura, T. Omori, and R. Kainuma, "Cryogenic superelasticity with large elastocaloric effect," NPG Asia Mater. **10**, e457 (2018).
[24]J. Xia, Y. Noguchi, X. Xu, T. Odaira, Y. Kimura, M. Nagasako, T. Omori, and R. Kainuma, "Iron-based superelastic alloys with near-constant critical stress temperature dependence," Science **369**, 855 (2020).
[25]H. C. Tong and C. M. Wayman, "Characteristic temperatures and other properties of thermoelastic martensites," Acta Metall. **22**, 887 (1974).
[26]T. Fukuda, T. Kakeshita, and Y.-H. Lee, "An interpretation of the kinetics of martensitic transformation in a $Ni_{45}Co_5Mn_{36.5}In_{13.5}$ alloy," Acta Mater. **81**, 121 (2014).
[27]K. Matsuura, Y. Nishizawa, M. Kriener, T. Kurumaji, H. Oike, Y. Tokura, and F. Kagawa, "Thermodynamic determination of the equilibrium first-order phase-transition line hidden by hysteresis in a phase diagram," Sci. Rep. **13**, 6876 (2023).
[28]J. Chen, W. Wang, F. Liu, B. Wei, L. Lei, G. Fang, R. O. Ritchie, and U. Ramamurty, "Functional fatigue and restoration in superelastic NiTi shape-memory alloys," Int. J. Plast. **194**, 104483 (2025).
[29]A. Seeger, "The temperature dependence of the critical shear stress and of work-hardening of metal crystals," Philos. Mag. **45**, 771 (1954).
[30]U. F. Kocks, A. S. Argon, and M. F. Ashby, *Progress in Materials Science*, edited by B. Chalmers, J. W. Christian, and T. B. Massalski (Pergamon Press, Oxford, 1975), Vol. 19.
[31]K. Niitsu, Y. Kimura, and R. Kainuma, "Transformation entropy change and precursor phenomena in Ni-rich Ti–Ni shape memory alloys," J. Mater. Res. **32**, 3822 (2017).
[32]R. Zarnetta, R. Takahashi, M. L. Young, A. Savan, Y. Furuya, S. Thienhaus, B. Maaß, M. Rahim, J. Frenzel, H. Brunken, Y. S. Chu, V. Srivastava, R. D. James, I. Takeuchi, G. Eggeler, and L. Ludwig, "Identification of quaternary shape memory alloys with near-zero thermal hysteresis and unprecedented functional stability," Adv. Funct. Mater. **20**, 1917 (2010).
[33]Y. Song, X. Chen, V. Dabade, T. W. Shield, and R. D. James, "Enhanced reversibility and unusual microstructure of a phase-transforming material," Nature **502**, 85 (2013).
[34]J. Cui, Y. S. Chu, O. O. Famodu, Y. Furuya, J. Hattrick-Simpers, R. D. James, A. Ludwig, S. Thienhaus, M. Wuttig, Z. Zhang, and I. Takeuchi, "Combinatorial search of thermoelastic shape-memory alloys with extremely small hysteresis width," Nat. Mater. **5**, 286 (2006).
[35]K. Niitsu, Y. Kimura, X. Xu, and R. Kainuma, "Composition dependences of entropy change and transformation temperatures in Ni-rich Ti–Ni system," Shape Mem. Superelasticity **1**(2), 124–131 (2015).